Hydrogen Transfer vs Proton Transfer in 7-Hydroxy-quinoline·(NH₃)₃: A CASSCF/CASPT2 Study

Antonio Fernández-Ramos,[†] Emilio Martínez-Núñez,[†] Saulo A. Vázquez,*,[†] Miguel A. Ríos,[†] Carlos M. Estévez,[‡] Manuela Merchán,[§] and Luis Serrano-Andrés*,[§]

Departamento de Química Física, Facultade de Química, Universidade de Santiago de Compostela, Santiago de Compostela, Spain, Departamento de Química Física, Facultade de Química, Universidade de Vigo, Vigo, Spain, and Unidad de Química Teórica, Instituto de Ciencia Molecular, Universitat de València, València, Spain

Multiconfigurational CASSCF and CASPT2 calculations were performed to investigate the enol → keto tautomerization in the lowest singlet excited state of the 7-hydroxyquinoline·(NH₃)₃ cluster. Two different reaction mechanisms were explored. The first one corresponds to that proposed previously by Tanner et al. (*Science* **2003**, *302*, 1736) on the basis of experimental observations and CASSCF optimizations under C_s-symmetry constraints. This mechanism comprises four consecutive steps and involves nonadiabatic transitions between the valence $^1\pi\pi^*$ state and a $\pi\sigma^*$ Rydberg-type state, resulting in hydrogen-atom transfer. Single-point CASPT2 calculations corroborate that for C_s-symmetry pathways hydrogen-atom transfer is clearly preferred over proton transfer. The second mechanism, predicted by CASSCF optimizations without constraints, implies proton transfer along a pathway on the $^1\pi\pi^*$ surface in which one or more ammonia molecules depart significantly from the molecular plane defined by the hydroxyquinoline ring. The results suggest that both mechanisms may be competitive with proton transfer being somewhat favorable over hydrogen-atom transfer.

I. Introduction

Proton transfer (PT) and hydrogen-atom transfer (HAT) reactions play a fundamental role in a variety of chemical and biological processes.[1–13] A comprehensive understanding of the mechanisms and dynamics of these reactions is, therefore, of great importance. However, research on PT and HAT reactions at the molecular level is in general very difficult because of the structural complexity, very short time scales, and solvent fluctuations involved in these processes. Some of the difficulties associated with bulk systems can be avoided by preparing small clusters of reactants and solvent molecules.[14–30] One example is that of 7-hydroxyquinoline·(NH₃)ₙ clusters[26–30] in which hydrogen-bonded molecular wires formed by *n* ammonia molecules are attached to 7-hydroxyquinoline (7HQ). The latter compound is a heteroaromatic scaffold molecule containing an O–H donor group and an N acceptor site located far enough to accommodate a small solvent wire.

Leutwyler and co-workers[26–34] extensively investigated HAT or PT along the ammonia wire in 7HQ·(NH₃)₃ using spectroscopic methods and ab initio calculations. In the electronic ground state (S₀) the tautomeric 7-ketoquinoline·(NH₃)₃ [7KQ·(NH₃)₃] form is predicted to be 8.6 kcal mol⁻¹ less stable than 7HQ·(NH₃)₃. Neither PT nor HAT has actually been observed for 7HQ·(NH₃)₃ in the electronic ground state. In the lowest singlet excited state (S₁) this energetic ordering is reversed; in other words, the O–H group has a more pronounced acidic character, whereas the basicity of the N atom becomes enhanced.

When 7HQ·(NH₃)₃ is excited to the S₁ origin (one π electron is promoted to a π^* molecular orbital), no reaction takes place but additional excitation of ammonia-wire vibrations triggers a fast enol ($^1\pi\pi^*$) → keto ($^1\pi\pi^*$) tautomerization with a reaction threshold of about 200 cm⁻¹.[26] In order to interpret these observations, Leutwyler and co-workers[26] performed molecular structure calculations for the S₁ and S₂ states using the configuration interaction singles (CIS)[35] and complete active space self-consistent field (CASSCF)[36,37] methods, concluding that after the S₁ ← S₀ excitation the enol → keto tautomerization proceeds via HAT (or coupled electron–proton transfer) rather than through PT. The whole (excited state) acid–base process comprises four consecutive H-atom translocations along the ammonia wire (see Figures 1 and 2)[26] in a way similar to the Grotthuss proton conduction mechanism in water.[38]

The interpretation of Leutwyler and co-workers[26] follows the mechanism of Domcke and Sobolewski proposed as a new paradigm of excited-state proton-transfer reactivity.[39] In this mechanism, inferred from CASSCF and CASPT2 calculations on phenol, pyrrol, indole, and their clusters with water and ammonia,[40–42] the key role is played by excited singlet states of $\pi\sigma^*$ nature (where σ^* is a Rydberg-type orbital), which have repulsive potential-energy surfaces with respect to the stretching of O–H or N–H bonds. For the particular case of 7HQ·(NH₃)₃, as the O–H bond stretches, the energy of the $^1\pi\pi^*$ state increases and soon this state crosses the $^1\pi\sigma^*$ state, which becomes more stable as the reaction progresses.[26] After a nonadiabatic transition to the $^1\pi\sigma^*$ state, the structure of 7HQ·(NH₃)₃ should be viewed as a radical pair (σ^* is a diffuse orbital centered on one of the N atoms of the ammonia wire) rather than as an ion pair, which would be the case if only the proton were transferred to the ammonia wire. In the final step of the

* To whom correspondence should be addressed. E-mail: qfsaulo@usc.es, Luis.Serrano@uv.es.
† Universidade de Santiago de Compostela.
‡ Universidade de Vigo.
§ Universitat de València.
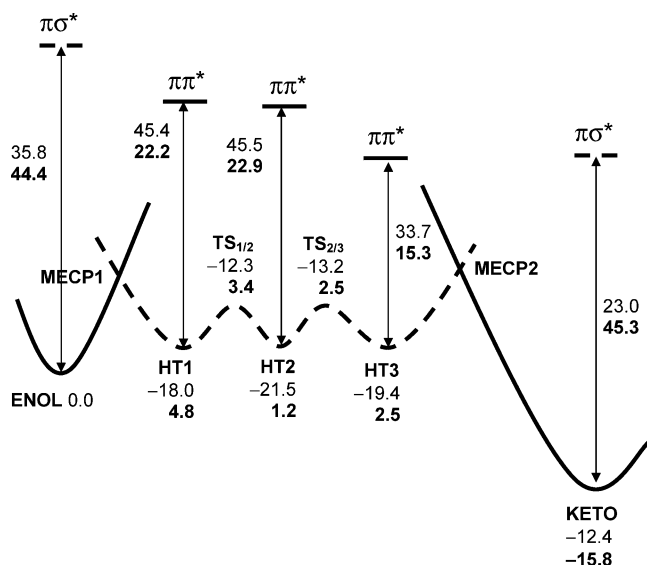
Figure 1. Qualitative schematic diagram of the energy profile for the enol → keto tautomerization in the S_1 excited state of $7KQ \cdot (NH_3)_3$, obtained by SA-3-CAS(12,12)/6-31(+)G(d,p) optimizations under C_s constraints. The solid lines correspond to the $\pi\pi^*$ state and the dashed line to the $^1\pi\sigma^*$ state. The plain and bold numbers are SA-5-CAS and MS-5-CASPT2 relative energies (in kcal/mol), respectively. HT1, HT2, and HT3 denote the intermediate species formed by consecutive H-atom translocations. The minimum energy crossing points MECP1 and MECP2 connect the ENOL/HT1 and HT3/KETO nonadiabatic transformations, respectively.
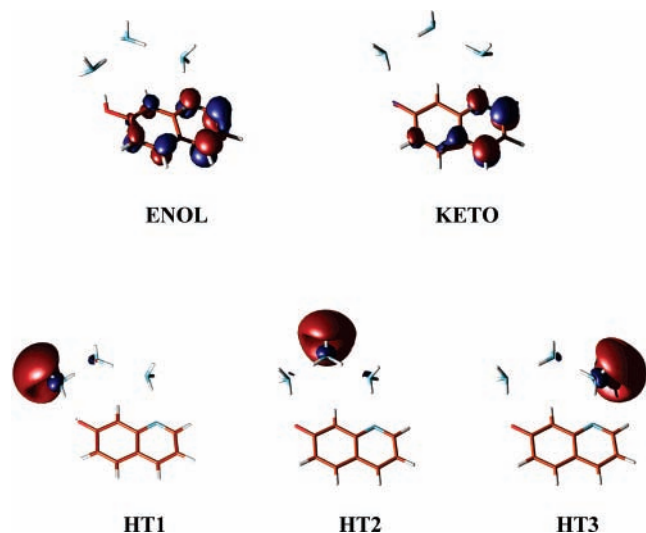
Figure 2. Structures of the minima along the HAT reaction profile showing the virtual molecular orbital that contributes mostly to the S_1 excited state.

enol → keto tautomerization a second curve crossing leads to $7KQ \cdot (NH_3)_3$ in the $^1\pi\pi^*$ state.

Very recently, Leutwyler and co-workers[34] performed ab initio CIS calculations to investigate the possible competition between HAT and PT in the $7HQ \cdot (NH_3)_3$ cluster. The latter process would take place if the dynamics occurs entirely on the $^1\pi\pi^*$ surface. They found a PT path that involves two synchronous proton transfers and lies 20−25 kcal/mol above the HAT path. Accordingly, they concluded that the PT path is closed for $7HQ \cdot (NH_3)_3$ (at the energies considered in their experiments[26,27]) but may become competitive with HAT in larger ammonia−solvent clusters.

It is important to remark that from the experimental results only it cannot be concluded whether the enol → keto tautomer-

ization proceeds via HAT or PT and that the interpretation of Leutwyler and co-workers is based on CIS and CASSCF calculations.[26] Two major concerns, however, may be raised about the reliability of these calculations and, as a consequence, of the above conclusion too. First, it is well known that, in general, these two ab initio methods do not render accurate energies because they lack most of the electronic correlation effects. Second, the CASSCF optimizations were carried out under C_s-symmetry constraints.[26] For pronounced nonplanar geometries, however, the scenario may be significantly different. In order to investigate more rigorously the possible competition between excited-state PT and HAT in the $7HQ \cdot (NH_3)_3$ cluster, we performed CASSCF optimizations with and without symmetry constraints and single-point multiconfigurational second-order perturbation theory calculations based on the CASSCF reference function (CASPT2).[43−45] The latter is a general quantum chemical method which has proved to be very accurate, particularly for excited-state calculations.[46−53]

II. Computational Methods

The optimizations without any symmetry constraints were performed at the CASSCF level using a state average procedure over the three lowest singlet states equally weighted (SA-3), relaxing subsequently the appropriate root. The standard 6-31G-(d,p) basis set was employed for geometry optimizations.[54] The active space consisted of 12 electrons in 11 active orbitals [CAS-(12,11)], which comprise the 6 valence π orbitals and the 5 valence π^* orbitals of the 7HQ ring. The energies of the $^1\pi\pi^*$ and $^1\pi\sigma^*$ states corresponding to the geometries of the stationary points obtained at the SA-3-CAS(12,11)/6-31G(d,p) level were then refined by single-point multistate (MS) CASPT2 calculations[55] using the respective SA-5-CAS wave functions as reference. For the calculations, correlated at the second order, two different basis sets were used: the standard 6-31++G-(d,p) basis set[56] and the 6-31G(d,p) basis set augmented with a set of diffuse s and p functions with the exponents ($\alpha_s = 0.015$ and $\alpha_p = 0.024$) derived by Leutwyler and co-workers previously.[26] The latter basis set will be denoted hereafter as 6-31-(+)G(d,p). Following the strategy employed by Leutwyler and co-workers,[26] we located these diffuse functions either on the N atom bearing the H atom that is being transferred (for minima on the potential-energy surface) or on the "moving" H atom (for transition states). The active orbitals for the SA-5-CAS and MS-5-CASPT2 calculations, with either the 6-31++G(d,p) or the 6-31(+)G(d,p) basis set, comprised the 11 π orbitals plus a σ^* Rydberg orbital.

The optimizations under C_s-symmetry constraints were performed at the SA-3-CAS(12,12)/6-31G(+)(d,p) level. The energies of the stationary points were then improved by MS-5-CASPT2(12,12)//SA-5-CAS(12/12)/6-31G(+)(d,p) calculations. All the CASPT2 calculations were carried out with an imaginary level shift of 0.2 au in order to prevent the effects of intruder states.[57] All the above computations were performed with the MOLCAS-6.2 quantum chemistry software.[58,59]

Additional calculations were carried out with the GAMESS[60] and MOLPRO[61] programs. GAMESS was used in preliminary single-state CAS(12,11)/6-31G(d) calculations, which included the evaluation of vibrational frequencies of the stationary points and minimum energy paths, necessary to characterize the nature of transition states and minima along the reaction coordinate and confirm that a particular transition state is the correct structure that links the corresponding minima. MOLPRO was employed to search for minimum energy crossing points (MECP) between the $^1\pi\pi^*$ and $^1\pi\sigma^*$ states in the C_s pathway.

Hydrogen Transfer vs Proton Transfer in 7HQ·(NH₃)₃

J. Phys. Chem. A, Vol. 111, No. 26, 2007 **5909**

III. Results and Discussion

A. Calculations under C_s-Symmetry Constraints. Figure 1 shows a schematic potential-energy profile for the enol($^1\pi\pi^*$) → keto($^1\pi\pi^*$) tautomerization obtained at the SA-5-CAS and MS-5-CASPT2 levels using SA-3-CAS/6-31(+)G(d,p) optimizations of the S₁ state under C_s-symmetry constraints using equal weights for the three lowest singlet states. Figure 2 depicts the structures of the minima associated with this profile as well as a representation of the π^* and σ^* molecular orbitals that contribute dominantly to the S₁ excited-state wave function. In this work we used the nomenclature given in ref 26 to name the stationary points along the HAT profile. Specifically, HT1, HT2, and HT3 denote the minima corresponding to the first, second, and third intermediate species formed, respectively, by consecutive H-atom translocations. In addition, TS$_{1/2}$ refers to the transition state that links HT1 and HT2, and TS$_{2/3}$ refers to the transition state of the consecutive step HT2 → HT3. The energies given in Figure 1 correspond to SA-5-CAS(12,12) and MS-5-CASPT2 single-point calculations performed on the minima and transition states (of the S₁ surface) optimized at the SA-3-CAS/6-31(+)G(d,p) level.

As expected, the present SA-CAS(12,12)/6-31(+)G(d,p) results are in agreement with the CAS(12,11)/6-31(+)G(d,p) calculations of Leutwyler and co-workers.[26] The S₁ state of the reactant (i.e., the enol form) is a $^1\pi\pi^*$ state, and its energy is predicted to be 36 kcal/mol lower than that of the lowest $^1\pi\sigma^*$ state at the SA-CAS(12,12) level. This energy difference is even higher at the MS-5-CASPT2 level (44 kcal/mol), at which the $^1\pi\sigma^*$ state corresponds to the third excited singlet state (S₃). However, as the O−H distance increases, the energy difference between these two states decreases, and when the proton approaches the ammonia molecule, the $^1\pi\sigma^*$ state becomes more stable than the $^1\pi\pi^*$ state. In HT1, the σ^* orbital is essentially located on the first ammonia molecule (see Figure 2), so that the nonadiabatic crossing between the $^1\pi\pi^*$ and $^1\pi\sigma^*$ states entails a charge-transfer process. In addition, since one proton and one electron have been transferred to the ammonia wire moiety, this process is more appropriately described as a HAT or a coupled electron−proton transfer than as a PT reaction. Our SA-CAS calculations predict that HT1 in the $^1\pi\sigma^*$ state is about 18 kcal/mol more stable than the enol form in the S₁-($^1\pi\pi^*$) state. In addition, for HT1 the SA-CAS energy of the S₂($^1\pi\pi^*$) state is ≈63 kcal/mol higher than that of the S₁($^1\pi\sigma^*$) state. Similar trends are found for the other two intermediate species (HT2 and HT3). At the MS-CASPT2 level, these energy differences change dramatically. In particular for HT1, the energy of the S₁($^1\pi\sigma^*$) state is now 4.8 kcal/mol above that of the enol form in the S₁($^1\pi\pi^*$) state, and the energy of the S₂-($^1\pi\pi^*$) state decreases to 17.4 kcal/mol with respect to that of the $^1\pi\sigma^*$ state. We found, therefore, that the CASSCF method favors the $^1\pi\sigma^*$ states much more than does the CASPT2 method, which is an expected result because dynamic correlation, introduced in this study through second-order perturbation theory, is in general more important for valence states than for Rydberg states.

It is interesting to notice that the MS-5-CASPT2 energetics of the stationary points do not follow the pattern predicted at the CASSCF level. More specifically, the relative energy of TS$_{1/2}$ (3.4 kcal/mol) is slightly smaller than that of HT1 (4.8 kcal/mol), and the relative energies of TS$_{2/3}$ and HT3 are equal to each other (2.5 kcal/mol). This might suggest that if the optimizations were done at the CASPT2 level, the number of steps comprising the whole acid−base process could be smaller (i.e., there may occur concerted HAT).

A central role in the HAT process is played by the conical intersections[27] between the $^1\pi\pi^*$ and the $^1\pi\sigma^*$ states, which facilitate nonadiabatic transitions between these two states. Searches for local minima on the crossing seams were performed at the CAS(12,12)/6-31(+)G(d,p) level, starting from the midpoints between the enol form and HT1, and between HT3 and the keto form. At this level of theory we located a MECP for the first step (enol → HT1, see Figure 1), but when we recalculated for this point the $^1\pi\pi^*$ and $^1\pi\sigma^*$ state energies at the MS-5-CASPT2/6-31(+)G(d,p) level, we found they differed significantly from each other (the $^1\pi\pi^*$ was favored). In order to obtain a better approximation to the MECP at the MS-5-CASPT2 level, we performed a linear interpolation between the CASSCF geometries of that point and HT1. In particular, for the midpoint of the interpolation, we found that the MS-5-CASPT2 energies of the $^1\pi\pi^*$ and $^1\pi\sigma^*$ states differed by only 2.8 kcal/mol. We considered the interpolated point as an approximation to the first crossing point (MECP1). Its geometry is very similar to that of HT1 with the N−H′ bond distance (H′ is the hydrogen transferred) equal to 1.112 Å (0.009 Å longer than in HT1). The energy of MECP1 relative to that of the enol form is estimated to be 5.6 kcal/mol (the absolute energy of MECP1 was calculated as the average of the $^1\pi\pi^*$ and $^1\pi\sigma^*$ state energies). Attempts were made to locate the second crossing point, but success was not achieved due to convergence problems. We then searched for a crossing point in the path obtained by linearly interpolating the geometries of HT3 and the product (the keto form), and we found a structure (MECP2) for which the MS-CASPT2 energies are equal to each other within 0.1 kcal/mol. The geometry of MECP2 is more similar to that of HT3 than to that of the keto form. The N−H′ bond distance (1.262 Å) is 0.146 Å longer than the corresponding bond distance in HT3. The energy of MECP2 relative to that of the enol form is 14.0 kcal/mol. This energy is significantly larger than those of the other relevant structures of this C_s pathway. This and the fact that the location of this crossing point was not done rigorously may suggest that this energy is overestimated.

All the results discussed so far involved 7HQ·(NH₃)₃ structures with C_s symmetry. The global energy barrier for the HAT process predicted by our CASPT2//CASSCF calculations is of the order of 5 kcal/mol if we do not consider MECP2. Because the optimizations were performed at the CASSCF level and the basis set employed may not be flexible enough for determining very accurate energies, we conclude that the energetics of the HAT C_s pathway may be consistent with the measured reaction threshold of only 0.6 kcal/mol. By contrast, a PT C_s pathway would involve energy barriers around 20 kcal/mol (at the CASPT2 level), and therefore, it would be energetically inaccessible at the very low excitation energies considered in the experiments.[26,27] Hence, the present CASPT2 calculations show that if the enol ($^1\pi\pi^*$) → keto ($^1\pi\pi^*$) tautomerization in 7HQ·(NH₃)₃ occurs through a C_s-symmetry (or close to C_s) pathway, the process would entail hydrogen-atom transfer, as concluded by Leutwyler and co-workers.[26] However, a crucial point here is whether the excited-state acid−base process in the 7HQ·(NH₃)₃ cluster takes place via C_s or nearly C_s pathways and, if this is not the case, whether PT can compete with HAT. Actually, the recent CIS calculations of Leutwyler and co-workers[34] show that, except for HT1, the stationary points of the HAT mechanism do not present C_s symmetry. In addition, most importantly, in the analysis of the vibronic S₁ ↔ S₀ spectra of the 7HQ·(NH₃)₃ and d_2-7DQ·(ND₃)₃ clusters, Leutwyler and co-workers[27] assigned two bands to intramolecular out-of-plane
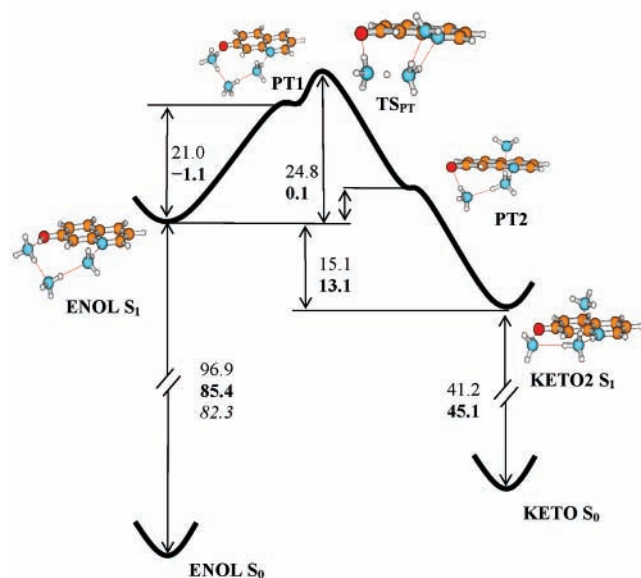
Figure 3. Qualitative schematic diagram of the energy profile for the enol → keto tautomerization in the S_1 excited state of 7KQ·$(NH_3)_3$, obtained by SA-3-CAS(12,11)/6-31G(d,p) optimizations without geometry constraints. The plain and bold numbers are SA-5-CAS/6-31++G(d,p) and MS-5-CASPT2/6-31++G(d,p) relative energies (in kcal/mol), respectively. The value in italic is the band origin of the spectrum[26] (see the text). The geometries of PT1 and PT2 were taken from the first steps of the corresponding optimizations (see text).

modes (in the S_1 state) that would be forbidden as fundamentals in C_s symmetry and are not observed in the closely related 7HQ·$(NH_3)_2$ cluster, which has C_s symmetry. As they stated, the appearance of these bands is a diagnostic sign for the lower (C_1) symmetry of the 7HQ·$(NH_3)_3$ cluster.

B. Calculations without Symmetry Constraints. The optimizations without any symmetry constraints were performed at the SA-3-CAS(12,11)/6-31G(d,p) level using as starting points the geometries of the stationary points located in preliminary single-state CASSCF(12,11)/6-31G(d) calculations. The active orbitals comprised all 11 valence π orbitals. Because the basis set does not include diffuse functions, the calculations led to valence states only. Figure 3 depicts the reaction profile on the $^1\pi\pi^*$ potential-energy surface predicted at this study together with drawings of the geometries of the relevant stationary points. Our preliminary CAS(12,11)/6-31G(d) calculations predicted that the tautomerization takes place through three consecutive proton-transfer steps: (1) from the enol form to the intermediate denoted as PT1 in the figure, (2) from this intermediate to a second intermediate denoted as PT2, and (3) from PT2 to the product designated as keto2. An energy minimum path calculation was carried out to ensure that TS_{PT} links PT1 and PT2. However, optimizations of the (preliminary) PT1 and PT2 structures at the SA-3-CAS(12,11)/6-31G(d,p) level led to the enol and keto2 forms, respectively. At this level of theory the PT reaction is more appropriately represented by a profile with only one transition state (TS_{PT}) and two shoulders associated to the PT1 and PT2 structures. We emphasize that the central issue here is not whether the PT process involves one or more elementary steps but whether the enol → keto tautomerization entails PT or HAT.

The geometry of the enol form in the S_1 state is similar to that in the ground electronic state, and the most notable feature is that the central ammonia molecule in the wire is markedly out of the plane defined by the 7HQ molecule. In TS_{PT}, two ammonia molecules are significantly separated from the molecular plane of the 7HQ ring. We notice that the PT pathway

TABLE 1: Relative Energies (kcal/mol) of the Three Lowest Singlet States Calculated for the Relevant Structures of the C_1 Pathway[a]

state	enol	PT1	TS_{PT}	PT2	keto2
	SA(5)-CASSCF(12,12)/6-31++G(d,p)				
S_0	0.0	33.3	46.6	44.0	29.8
	0.0	*38.3*	*51.2*	*49.6*	*35.7*
S_1	86.1 ($\pi\pi^*$)	94.4 ($\pi\sigma^*$)	101.8 ($\pi\sigma^*$)	94.6 ($\pi\sigma^*$)	71.0 ($\pi\pi^*$)
	86.1	*91.9*	*98.3*	*93.0*	*76.7*
S_2	119.5 ($\pi\pi^*$)	107.1 ($\pi\pi^*$)	110.9 ($\pi\pi^*$)	95.6 ($\pi\pi^*$)	105.3 ($\pi\sigma^*$)
	123.5	*111.8*	*114.8*	*100.3*	*106.5*
	MS(5)-CASPT2(12,12)/6-31++G(d,p)				
S_0	0.0	15.8	22.8	24.4	19.1
	0.0	*13.2*	*20.8*	*23.7*	*18.2*
S_1	77.3 ($\pi\pi^*$)	76.3 ($\pi\pi^*$)	77.5 ($\pi\pi^*$)	70.6 ($\pi\pi^*$)	64.2 ($\pi\pi^*$)
	78.2	*73.6*	*74.9*	*69.8*	*62.9*
S_2	100.6 ($\pi\pi^*$)	95.0 ($\pi\sigma^*$)	98.1 ($\pi\sigma^*$)	96.9 ($\pi\sigma^*$)	104.6 ($\pi\pi^*$)
	98.2	*87.2*	*90.5*	*91.3*	*103.1*

[a] Geometries obtained by SA(3)-CASSCF(12,11)/6-31G(d,p) optimizations, relaxing the second root (i.e., S_1). The character of the excited state is given in parentheses. Values in italic correspond to calculations using the 6-31(+)G(d,p) basis set. The geometries of PT1 and PT2 were taken from the first steps of the corresponding optimizations (see text).

found in this study is different from that predicted previously[34] by CIS calculations (see ref 34 for details).

To obtain accurate energies we performed single-point MS-5-CASPT2(12,12) calculations using SA-5-CAS(12,12) reference functions and the 6-31(+)G(d,p) and 6-31++G(d,p) basis sets. In these computations we also included one σ^* Rydberg molecular orbital in the active space in order to explore the importance of $^1\pi\sigma^*$ states. The energies of the lowest $^1\pi\pi^*$ and $^1\pi\sigma^*$ states obtained at the CASSCF and CASPT2 levels for the relevant structures are presented in Table 1. For completeness, we also show the energies of the PT1 and PT2 structures taken from the initial steps in the corresponding optimizations. As expected, both the SA-CASSCF and the MS-CASPT2 methods predict that the S_1 states of the reactant (enol form) and product (keto2) correspond to $^1\pi\pi^*$ excitations. The vertical excitation energy obtained by MS-CASPT2/6-31++G(d,p) calculations, using the ground-state-optimized geometry of the enol form, is 85.4 kcal/mol (see Figure 3), which is quite close to the value of 28 798.4 cm^{-1} (82.3 kcal/mol) corresponding to the origin of the S1 ← S0 two-color resonant two-photon ionization spectrum of the 7HQ·$(NH_3)_3$ cluster.[26] At the SA-CASSCF level, the S_1 state for the TS_{PT}, PT1, and PT2 structures is the $^1\pi\sigma^*$ Rydberg state, whereas the $^1\pi\pi^*$ valence state is S_2. However, this order is reversed at the MS-CASPT2 level, and in particular for TS_{PT}, the MS-5-CASPT2/6-31++G(d,p) energy difference between the two states (S_1 and S_2) is 20.6 kcal/mol, favoring the $^1\pi\pi^*$ valence state. With the 6-31(+)G-(d,p) basis set the energy difference is somewhat smaller but significant (15.6 kcal/mol). Therefore, for the C_1-symmetry pathway predicted in this study, excited-state PT is clearly preferred over HAT. Moreover, the MS(5)-CASPT2 calculations predict an essentially barrierless PT process as the energy of the transition state relative to that of enol (S_1) is calculated to be only 0.1 kcal/mol, which is consistent with the reaction threshold determined experimentally (0.6 kcal/mol).

An important issue about the experimental observation of the excited-state acid−base reaction in 7HQ·$(NH_3)_3$ concerns the enol → keto tautomerization yield, which is found to be ≤40%.[34] In addition, Leutwyler and co-workers[34] observed that the sum of enol and keto fluorescence drops to about 40% at an excess energy of 187 cm^{-1} (≈0.5 kcal/mol) and remains approximately stable up to the highest energies measured. In order to interpret

Hydrogen Transfer vs Proton Transfer in 7HQ·(NH$_3$)$_3$

J. Phys. Chem. A, Vol. 111, No. 26, 2007 **5911**

these observations, Leutwyler and co-workers[34] performed additional CIS calculations and found triplet states crossing the S$_1$ state in the HT1 and HT3 wells. They concluded that intersystem crossing to one of these triplet states and subsequent relaxation toward the enol side may lead to a loss of one or two ammonia molecules due to the excess energy (see ref 34 for details); as a consequence, the species will not be detectable on the mass channel of 7HQ·(NH$_3$)$_3$.[62] In this work, we have not explored this possibility but suggest a different plausible mechanism for the loss of one ammonia molecule. This is based on the geometries of the transition state (TS$_{PT}$) and product (keto2, see Figure 3) and on the potential-energy profile of the (C_1-symmetry) PT process, which shows a reverse barrier of ≈13 kcal/mol. As the reaction progresses from TS$_{PT}$ to keto2, the two first ammonia molecules approach the 7HQ molecular plane and the third ammonia molecule separates from this plane. This movement may take place quite rapidly because the reverse barrier is significant. Most of the excess energy may be transferred to vibrational excitation of ammonia wire modes, and in particular, a significant fraction of it may be deposited in the intramolecular NH···NH$_3$ stretching mode (where NH$_3$ is the out-of-plane ammonia molecule). The interaction energy between the ammonia molecule and the 7KQ·(NH$_3$)$_2$ moiety in keto2 is calculated to be 4.5 kcal/mol after correction for basis set superposition error. If zero-point energy effects were taken into account, this interaction energy could be reduced by about 1 kcal/mol.[63] Therefore, it is reasonable to expect that a significant part of the clusters lose one ammonia molecule if in fact the reaction profile of the tautomerization resembles that depicted in Figure 3.

Finally, it is also important to notice that the ammonia wire makes the 7HQ·(NH$_3$)$_3$ cluster a very "floppy" system. Actually, the C_s and C_1 structures of the enol form in the $^1\pi\pi^*$ state are predicted to be essentially isoenergetic. As a consequence, the ammonia wire may experience large-amplitude vibrations which might facilitate competition between hydrogen-atom transfer and proton transfer.

IV. Conclusions

The excited-state enol→keto tautomerization of 7-hydroxyquinoline·(NH$_3$)$_3$ was investigated by multiconfigurational CASSCF and CASPT2 calculations. The CASPT2 results corroborates that the C_s pathway on the S$_1$ surface involves nonadiabatic transitions between the $^1\pi\pi^*$ and $^1\pi\sigma^*$ states and, as a consequence, hydrogen-atom (or coupled electron−proton) transfer. The global energy barrier associated with this pathway is predicted to be about 5 kcal/mol by MS-CASPT2, which is in reasonable agreement with the experimental threshold of 0.6 kcal/mol. Proton transfer across the C_s pathway entails higher energies (≈20 kcal/mol higher), and therefore, it is not accessible at the excitation energies considered in the experiment.[26,27] In this regard, the CASPT2 results are in qualitative agreement with the CASSCF calculations of Leutwyler and co-workers, although quantitatively the energy differences between the valence and Rydberg states differ substantially with respect to those calculated at the CASSCF level. As expected, inclusion of dynamic correlation has more of a stabilizing effect on the valence states than it does on the Rydberg states.

The calculations performed without any geometrical constraints provided a completely different mechanistic picture of the acid−base process in the 7HQ·(NH$_3$)$_3$ cluster. According to the MS-CASPT2 calculations, the tautomerization along the calculated C_1 pathway, in which one or more ammonia molecules are markedly out of the plane defined by the 7HQ ring, proceeds with essentially no barrier, which is in line with the observations. The tautomerization takes place via proton transfer and probably by a single step. For the transition structure (TS$_{PT}$) the energy of the S$_2$($^1\pi\sigma^*$) state is significantly higher than that of the $^1\pi\pi^*$ state, and therefore, the $^1\pi\sigma^*$ surface should be inaccessible at the experimental conditions.[26,27] Interestingly, the CASSCF calculations still predict crossings between the valence and Rydberg states. In this case, inclusion of dynamic correlation is crucial to obtain not only quantitative but also qualitative results.

Whereas our calculations predict that the C_s and C_1 structures of the enol form have nearly the same energy, the experimental observations of Leutwyler and co-workers show that the 7HQ·(NH$_3$)$_3$ cluster is nonplanar. The ammonia wire makes the 7HQ·(NH$_3$)$_3$ cluster a very floppy system, and large-amplitude vibrations (of the ammonia wire) might promote competition between PT and HAT. Overall, the calculations suggest that proton transfer is preferred over hydrogen-atom transfer in the excited-state tautomerization of 7-hydroxyquinoline·(NH$_3$)$_3$.

Supporting Information Available: Cartesian coordinates and energies. This material is available free of charge via the Internet at http://pubs.acs.org.

References and Notes

(1) Douhal, A.; Kim, S. K.; Zewail, A. H. *Nature* **1995**, *378*, 260−263.

(2) Gutman, M.; Nachliel, E. *Annu. Rev. Phys. Chem.* **1997**, *48*, 329−356.

(3) Lu, D.; Voth, G. A. *J. Am. Chem. Soc.* **1998**, *120*, 4006−4014.

(4) Cukier, R. I.; Nocera, D. G. *Annu. Rev. Phys. Chem.* **1998**, *49*, 337−369.

(5) Vuilleumier, R.; Borgis, D. *J. Phys. Chem. B* **1998**, *102*, 10446−10458.

(6) Marx, D.; Tuckerman, M. E.; Hutter, J.; Parrinello, M. *Nature* **1999**, *397*, 601−604.

(7) Agarwal, P. K.; Webb, S. P.; Hammes-Schiffer, S. *J. Am. Chem. Soc.* **2000**, *122*, 4803−4812.

(8) Geissler, P. L.; Dellago, C.; Chandler, D.; Hutter, J.; Parrinello, M. *Science* **2001**, *291*, 2121−2124.

(9) Lill, M. A.; Helms, V. *Proc. Natl. Acad. Sci. U.S.A.* **2002**, *99*, 2778−2781.

(10) Cui, Q.; Karplus, M. *J. Phys. Chem. B* **2002**, *106*, 7927−7947.

(11) Pomès, R.; Roux, B. *Biophys. J.* **2002**, *82*, 2304−2316.

(12) Hynes, J. T.; Tran-Thi, T.-H.; Granucci, G. *J. Photochem. Photobiol. A* **2002**, *154*, 3−11.

(13) Rini, M.; Magnes, B.-Z.; Pines, E.; Nibbering, E. T. J. *Science* **2003**, *301*, 349−352.

(14) Cheshnovsky, O.; Knochenmuss, R.; Leutwyler, S. *Chem. Phys. Lett.* **1988**, *144*, 317−323.

(15) Held, A.; Pratt, D. W. *J. Am. Chem. Soc.* **1993**, *115*, 9708−9717.

(16) Lahmani, F.; Douhal, A.; Breheret, E.; Zehnacker-Rentien, A. *Chem. Phys. Lett.* **1994**, *220*, 235−242.

(17) Zwier, T. S. *Annu. Rev. Phys. Chem.* **1996**, *47*, 205−241.

(18) Nakajima, A.; Hirano, M.; Hasumi, R.; Kaya, K.; Watanabe, H.; Carter, C. C.; Williamson, J. M.; Miller, T. A. *J. Phys. Chem. A* **1997**, *101*, 392−398.

(19) Matsumoto, Y.; Ebata, T.; Mikami, N. *J. Chem. Phys.* **1998**, *109*, 6303−6311.

(20) Bach, A.; Leutwyler, S. *Chem. Phys. Lett.* **1999**, *299*, 381−388.

(21) Bach, A.; Coussan, S.; Müller, A.; Leutwyler, S. *J. Chem. Phys.* **2000**, *112*, 1192−1203.

(22) Folmer, D. E.; Wisniewski, E. S.; Stairs, J. R.; Castleman, A. W., Jr. *J. Chem. Phys. A* **2000**, *104*, 10545−10549.

(23) Yokohama, H.; Watanabe, H.; Omi, T.; Ishiuchi, S.; Fujii, M. *J. Chem. Phys. A* **2001**, *105*, 9366−9374.

(24) David, O.; Dedonder-Lardeux, C.; Jouvet, C. *Int. Rev. Phys. Chem.* **2002**, *21*, 499−523.

(25) Matsumoto, Y.; Ebata, T.; Mikami, N. *J. Chem. Phys. A* **2002**, *106*, 5591−5599.

(26) Tanner, C.; Manca, C.; Leutwyler, S. *Science* **2003**, *302*, 1736−1739.

(27) Manca, C.; Tanner, C.; Coussan, S.; Bach, A.; Leutwyler, S. *J. Chem. Phys.* **2004**, *121*, 2578−2590.

(28) Bach, A.; Leutwyler, S. *J. Chem. Phys.* **2000**, *112*, 560−565.

(29) Meuwly, M.; Bach, A.; Leutwyler, S. *J. Am. Chem. Soc.* **2001**, *123*, 11446−11453.

(30) Bach, A.; Tanner, C.; Manca, C.; Frey, H.-M.; Leutwyler, S. *J. Chem. Phys.* **2003**, *119*, 5933−5942.

(31) Tanner, C.; Manca, C.; Leutwyler, S. *Chimia* **2004**, *58*, 234−236.

(32) Manca, C.; Tanner, C.; Leutwyler, S. *Chimia* **2004**, *58*, 287−290.

(33) Coussan, S.; Meuwly, M.; Leutwyler, S. *J. Chem. Phys.* **2001**, *114*, 3524−3534.

(34) Tanner, C.; Manca, C.; Leutwyler, S. *J. Chem. Phys.* **2005**, *122*, 204326/1−204326/11.

(35) Foresman, J. B.; Head-Gordon, M.; Pople, J. A.; Frish, M. J. *J. Phys. Chem.* **1992**, *96*, 135−149.

(36) Roos, B. O.; Taylor, P. R.; Siegbahn, P. E. M. *Chem. Phys.* **1980**, *48*, 157−173.

(37) Roos, B. O. *Adv. Chem. Phys.* **1987**, *69*, 399−445.

(38) von Grotthuss, C. J. D. *Ann. Chim.* **1806**, *58*, 54.

(39) Domcke, W.; Sobolewski, A. L. *Science* **2003**, *302*, 1693−1694.

(40) Sobolewski, A. L.; Domcke, W. *Chem. Phys. Lett.* **2000**, *321*, 479−484.

(41) Sobolewski, A. L.; Domcke, W. *J. Phys. Chem. A* **2001**, *105*, 9275−9283.

(42) Sobolewski, A. L.; Domcke, W.; Dedonder-Lardeux, C.; Jouvet, C. *Phys. Chem. Chem. Phys.* **2002**, *4*, 1093−1100.

(43) Roos, B. O.; Linse, P.; Siegbahn, P. E. M.; Blomberg, M. R. A. *Chem. Phys.* **1982**, *66*, 197−207.

(44) Andersson, K.; Malmqvist, P. Å.; Roos, B. O.; Sadlej, A. J.; Wolinski, K. *J. Phys. Chem.* **1990**, *94*, 5483−5488.

(45) Andersson, K.; Malmqvist, P. Å.; Roos, B. O. *J. Chem. Phys.* **1992**, *96*, 1218−1226.

(46) Serrano-Andrés, L.; Merchán, M.; Nebot-Gil, I.; Lindh, R.; Roos, B. O. *J. Chem. Phys.* **1993**, *98*, 3151−3162.

(47) Serrano-Andrés, L.; Merchán, M.; Nebot-Gil, I.; Roos, B. O.; Fülscher, M. P. *J. Am. Chem. Soc.* **1993**, *115*, 6184−6197.

(48) Roos, B. O.; Andersson, K.; Fülscher, M. P.; Malmqvist, P. Å.; Serrano-Andrés, L.; Pierloot, K.; Merchán, M. Multiconfigurational perturbation theory: Applications in electronic spectroscopy. In *Advances in Chemical Physics: New Methods in Computational Quantum Mechanics*; Prigogine, I., Rice, S. A., Eds.; John Wiley & Sons: New York, 1996; Vol. XCIII, pp 219−331.

(49) Serrano-Andrés, L.; Forsberg, N.; Malmqvist, P. Å. *J. Chem. Phys.* **1998**, *108*, 7202−7216.

(50) Serrano-Andrés, L.; Merchán, M. Spectroscopy: Applications. In *Encyclopedia of Computational Chemistry*; Schleyer, P. v. R., et al., Eds.; Wiley: Chichester, 2004.

(51) Merchán, M.; Serrano-Andrés, L. Ab Initio methods for excited states. In *Computational Photochemistry*; Elsevier: Amsterdam, 2005.

(52) Merchán, M.; Serrano-Andrés, L.; Robb, M. A.; Blancafort, L. *J. Am. Chem. Soc.* **2005**, *127*, 1820.

(53) Azizi, Z.; Roos, B. O.; Veryazov, V. *Phys. Chem. Chem. Phys.* **2006**, *8*, 2727−2732.

(54) Binkley, J. S.; Pople, J. A.; Hehre, W. J. *J. Am. Chem. Soc.* **1980**, *102*, 939−947.

(55) Finley, J.; Malmqvist, P. Å.; Roos, B. O.; Serrano-Andrés, L. *Chem. Phys. Lett.* **1998**, *288*, 299−306.

(56) Frisch, M. J.; Pople, J. A.; Binkley, J. S. *J. Chem. Phys.* **1984**, *80*, 3265−3269.

(57) Forsberg, N.; Malmqvist, P.-Å. *Chem. Phys. Lett.* **1997**, *274*, 196−204.

(58) Veryazov, V.; Widmark, P.-O.; Serrano-Andrés, L.; Lindh, R.; Roos, B. O. *Int. J. Quantum Chem.* **2004**, *100*, 626−635.

(59) Andersson, K.; Barysz, M.; Bernhardsson, A.; Blomberg, M. R. A.; Carissan, Y.; Cooper, D. L.; Fülscher, M. P.; Gagliardi, L.; de Graaf, C.; Hess, B. A.; Hagberg, D.; Karlström, G.; Lindh, R.; Malmqvist, P.-Å.; Nakajima, T.; Neográdi, P.; Olsen, J.; Raab, J.; Roos, B. O.; Ryde, U.; Schimmelpfennig, B.; Schütz, M.; Seijo, L.; Serrano-Andrés, L.; Siegbahn, P. E. M.; Stålring, J.; Thorsteinsson, T.; Veryazov, V.; Widmark, P.-O. *MOLCAS,* Version 6.2. Department of Theoretical Chemistry, Chemistry Center, University of Lund: Lund, Sweden, 2005.

(60) Schmidt, M. W.; Baldridge, K. K.; Boatz, J. A.; Elbert, J. A.; Gordon, M. S.; Jensen, J. H.; Koseki, S.; Matsunaga, N.; Gguyen, K. A.; Su, S. J.; Windus, T. L.; Dupuis, M.; Montgomery, J. A. *J. Comput. Chem.* **1993**, *12*, 1347−1363.

(61) Werner, H.-J.; Knowles, P. J.; Lindh, R.; Manby, F. R.; Schütz, M.; Celani, P.; Korona, T.; Rauhut, G.; Amos, R. D.; Bernhardsson, A.; Berning, A.; Cooper, D. L.; Deegan, M. J. O.; Dobbyn, A. J.; Eckert, F.; Hampel, C.; Hetzer, G.; Lloyd, A. W.; McNicholas, S. J.; Meyer, W.; Mura, M. E.; Nicklass, A.; Palmieri, P.; Pitzer, R.; Schumann, U.; Stoll, H.; Stone, A. J.; Tarroni, R.; Thorsteinsson, T. *MOLPRO,* version 2002.6, 2002.

(62) The detection technique used in the experiments of Leutwyler and co-workers involves ionization of the excited clusters followed by analysis of the cluster ions in a time-of-flight mass spectrometer.

(63) Altmann, J. A.; Govender, M. G.; Ford, T. A. *Mol. Phys.* **2005**, *103*, 949−961.